

Single-Longitudinal-Mode Pulsed LiF:F₂⁻ Color-Center Laser for High Resolution Spectroscopy

T. T. Basiev¹, A. G. Papashvili¹, V. V. Fedorov¹, S. V. Vassiliev¹, and W. Gellermann²

¹ Laser Materials and Technology Research Center, General Physics Institute of RAS,
 Vavilova 38 Block “D,” GSP-1, 117942 Moscow, Russia

e-mail: vasia@kapella.gpi.ru

² University of Utah, Department of Physics, JFB-312, Salt Lake City, Utah, USA

Received April 1, 2003

Abstract—The pulsed LiF:F₂⁻ color-center laser with a grazing incidence grating cavity was investigated theoretically and experimentally. The SLM laser operation with an efficiency of about 1% was achieved. A novel scheme for the high-power narrowband color-center laser was proposed.

1. INTRODUCTION

At the present moment, the various schemes of the grazing incidence grating cavity (GIG or Littman–Metcalf scheme [1]) are in wide use in dye lasers, Ti:sapphire lasers, diode lasers, and other types of tunable laser techniques [2, 3]. The main advantages of the grazing incidence grating cavity are high spectral selectivity, simple construction, and ease of control.

In this paper are presented the results of a theoretical and experimental investigation of the LiF:F₂⁻ color-center laser with a GIG cavity. The theoretical model of the laser makes it possible to determine the parameters of the laser cavity providing single-longitudinal-mode (SLM) laser operation. On the basis of the theoretical results, the SLM color-center laser with a grazing incidence grating cavity was built and studied. With the standard Littman–Metcalf cavity scheme, the laser efficiency was about 1% while Nd:YAG laser pumping with a pump pulse energy of about 20 mJ and a pulse duration of about 20 ns was used.

To improve the laser characteristics, various cavity configurations and pumping schemes were experimentally investigated. As a result, a novel scheme for the high-power narrowband color-center laser was proposed. Our experiments have shown that, for the novel cavity scheme, considerable laser efficiency and spectral selectivity could be reached.

2. MODELING OF THE LiF:F₂⁻ COLOR-CENTER LASER WITH A GIG CAVITY

2.1. Model Description

A schematic of the GIG cavity color-center laser is shown in Fig. 1. The laser cavity consists of the back mirror M1, tuning mirror M2, and the diffraction grating G in a grazing incidence mounting. The pump radiation P couples in the laser crystal C via the dichroic mirror M1. The spectral selectivity of the cavity can be

improved by using the intra-cavity beam expander E and etalon F [4, 5]. The laser operation wavelength λ_0 is determined by the well-known diffraction grating formula

$$\lambda_0 = \Lambda(\sin \theta + \sin \varphi), \quad (1)$$

where Λ is the grating period and θ and φ are the grazing incidence and diffraction angles. Usually, the tuning of the GIG laser wavelength is carried out by varying the angle φ (mirror M2 rotation).

The dispersive properties of the GIG cavity were estimated in the geometrical optics approximation. In Fig. 2 is shown the GIG cavity with the laser crystal removed and the M1 mirror replaced by the pin hole. Let us consider propagation of a Gaussian beam with frequency deviation $\delta\nu$ from the central wavelength λ_0 in this optical system. Let the pin-hole transmission t be determined by the relation

$$t(y, z) = \exp\left(-\frac{y^2 + z^2}{R^2}\right), \quad (2)$$

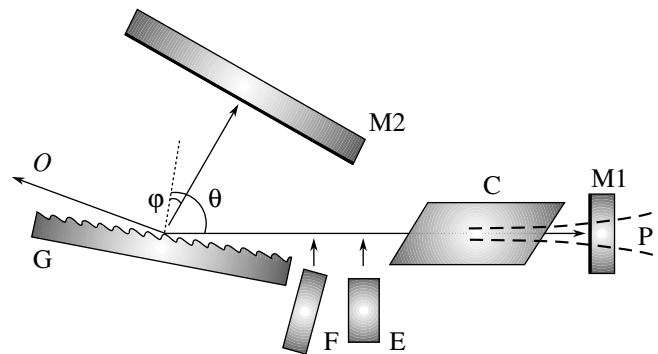


Fig. 1. Schematic of the color-center laser with a GIG cavity.

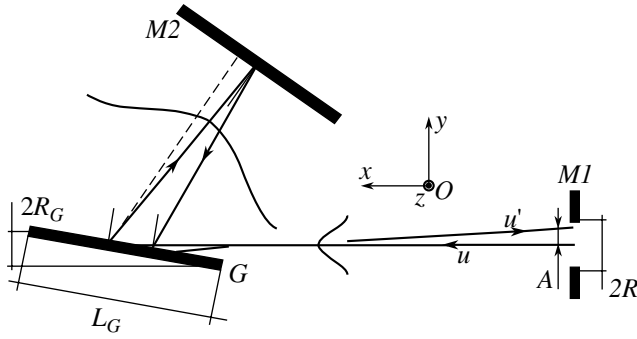


Fig. 2. Schematic for estimation of GIG cavity transmission.

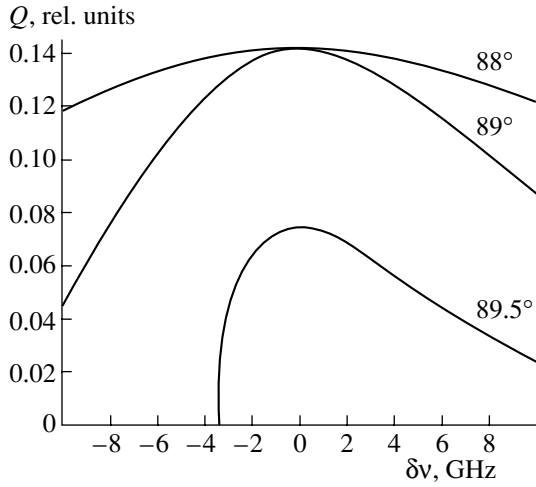


Fig. 3. GIG cavity roundtrip transmission Q vs. frequency detuning $\delta\nu$ (for different values of grating incidence angle θ).

where R is the effective pin-hole radius and the initial distribution of the beam intensity at the pin-hole plane is given by

$$u(x=0, y, z) = \frac{1}{\pi R^2} \exp\left(-\frac{y^2 + z^2}{R^2}\right). \quad (3)$$

The beam parameters after the cavity roundtrip could be described by the following expression:

$$u(x=0, y, z) = T_G E_G^2 \frac{1}{\pi R_y' R_z'} \exp\left[-\frac{(y-A)^2}{R_y'^2} - \frac{z^2}{R_z'^2}\right]. \quad (4)$$

The factor A depends on the frequency detuning $\delta\nu$ and characterizes the deviation of the beam position from the cavity axis. The beam transverse size changes due to its natural divergence. Moreover, the strong expan-

sion of the beam in the Oxy plane takes place because of the diffraction at the grating. Thus,

$$\begin{aligned} R_z' &\sim L^{(\text{cav})} \delta\theta, \\ R_y' &\sim L^{(M1-G)} \delta\theta, \end{aligned} \quad (5)$$

where $\delta\theta \sim \lambda_0/R$ is the beam divergence angle, $L^{(\text{cav})}$ is the cavity length, and $L^{(M1-G)}$ is the pin-hole–grating distance. If the grating input aperture $2R_G = L_G \cos\theta$ is smaller than the initial transverse size of the beam, then the part of the beam bypasses the grating. These additional losses are taken into account in Eq. (4) by factor T_G . Factor E_G in Eq. (4) characterizes the grating diffraction efficiency. The roundtrip transmission of the cavity can be found from Eqs. (2) and (4):

$$\begin{aligned} Q &= \iint tu' dy dz \\ &= T_G E_G^2 \frac{R^2}{R^2 + R_y'^2} \frac{R^2}{R^2 + R_z'^2} \exp\left(-\frac{A^2}{R^2 + R_y'^2}\right). \end{aligned} \quad (6)$$

In Fig. 3 is shown the cavity transmission Q as a function of the frequency detuning $\delta\nu$. Calculations were made for the cavity length $L^{(\text{cav})} = 15$ cm, grating length $L_G = 6$ cm, pin-hole diameter $2R = 1$ mm, and different values of grating incidence angle θ . It was supposed that the grating diffraction efficiency was equal to 100% ($E_G = 1$). As shown, the cavity spectral selectivity increases rapidly as the grating incidence angle increases. For $\theta = 89.5^\circ$, the spectral width of the cavity transmission contour became comparable with the cavity mode space ($\delta\nu^{(\text{cav})} = c/2L^{(\text{cav})} \approx 1$ GHz). However, for such a close-to-limit incidence angle, the grating input aperture ($2R_G = L_G \cos\theta \approx 0.5$ mm) became smaller than the pin-hole diameter, which leads to additional losses.

The model of the color-center laser with a dispersive cavity was built on the basis of a 0D approximation; i.e., the averaged on the cavity length parameters of the active medium and the laser radiation were considered. This approximation is usual for the color-center laser modeling and makes it possible to obtain qualitative and quantitative estimations of the laser characteristics [6].

The equations describing the laser action in the 0D approximation are the following:

$$\begin{aligned} \dot{n} &= (N\sigma_p^{(01)} - n(\sigma_p^{(01)} + \sigma_p^{(10)}))F_p \\ &+ (N\sigma_L^{(01)} - n(\sigma_L^{(01)} + \sigma_L^{(10)}))F_L - \frac{n}{\tau}, \\ \dot{F}_L &= c \frac{L_C}{L^{(\text{cav})}} \left[(-N\sigma_L^{(01)} + n(\sigma_L^{(01)} + \sigma_L^{(10)}) - k_L)F_L \right. \\ &\quad \left. + \omega \frac{n}{\tau} \right] - \gamma F_L, \end{aligned} \quad (7)$$

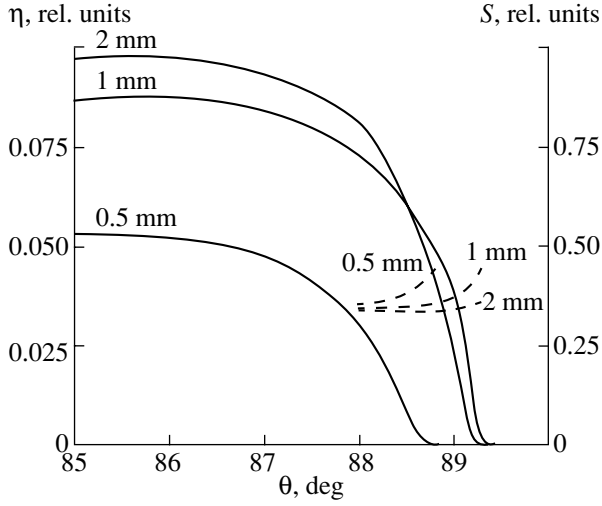


Fig. 4. Color-center laser efficiency η and line-width factor S vs. grating incidence angle θ (for different diameters of the active region).

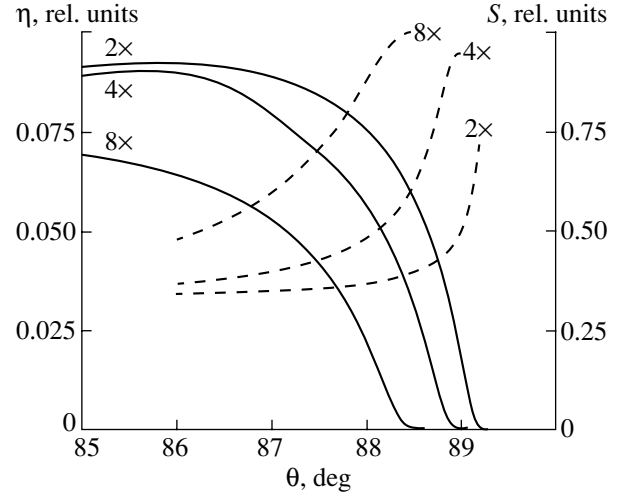


Fig. 5. Color-center laser efficiency η and line-width factor S vs. grating incidence angle θ (for different intracavity expander magnifications).

where c is the light velocity [cm s^{-1}], N is the concentration of active centers in the laser crystal [cm^{-3}], n is the upper laser level population [cm^{-3}], F_L is the flow density of laser radiation photons [$\text{cm}^{-2} \text{s}^{-1}$], F_P is the flow density of pump radiation photons [$\text{cm}^{-2} \text{s}^{-1}$], $\sigma_\alpha^{(\beta)}$ are the effective cross section of the stimulated transitions [cm^2] (the wavelength of transition is denoted by subscript, and direction of the transition is denoted by superscript), K_α are the parasitic losses in the laser crystal [cm^{-1}], τ is the characteristic time of spontaneous decay of the upper laser level [s], L_C is the laser crystal length [cm], $L^{(\text{cav})}$ is the cavity length [cm], parameter γ characterizes the cavity losses, and parameter ω characterizes the origin of the laser emission. The averaged pump intensity F_P can be approximated by the relation

$$F_P = F_P^{(0)} [1 - \exp(-\alpha)] / \alpha, \quad (8)$$

where

$$\alpha = L_C (N \sigma_P^{(01)} - n (\sigma_P^{(01)} + \sigma_P^{(10)}) + k_P) \quad (9)$$

and $F_P^{(0)}$ is the pump intensity at the laser crystal input end. The parameter γ is determined by the relation

$$\gamma = -\frac{c}{2L^{(\text{cav})}} \ln Q, \quad (10)$$

where Q is the cavity feed-back factor. The temporal shape of the laser pulse is given by

$$F_L^{(\text{out})}(t) = \frac{1}{2} T F_L, \quad (11)$$

where T is the transmission of the cavity out coupler.

To simulate the narrowing of the laser emission in the dispersive cavity, Eqs. (7) were solved simultaneously for three spectral components: the principal cavity frequency (see Eq. (1)) and two neighboring longitudinal modes (frequency deviation $\delta\nu = c/2L^{(\text{cav})}$). The cavity losses for each spectral component were calculated from Eq. (6). The experimentally measured values of the diffraction grating efficiency were used for simulations (see Fig. 7). The spectral line width of the laser emission was characterized by factor S :

$$S = E_0 / (E_{-\delta\nu} + E_0 + E_{+\delta\nu}), \quad (12)$$

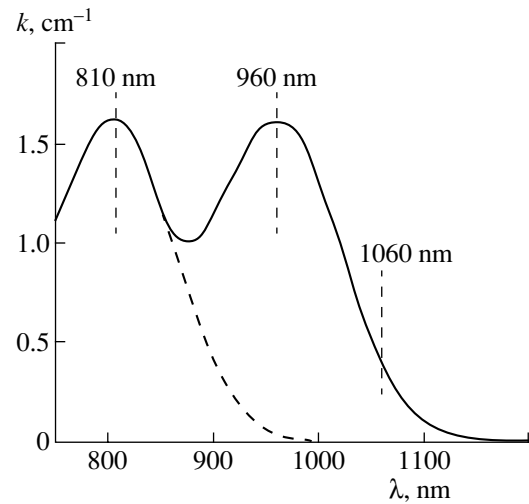


Fig. 6. Absorption spectra of the LiF:F₂⁻ color-center crystal.

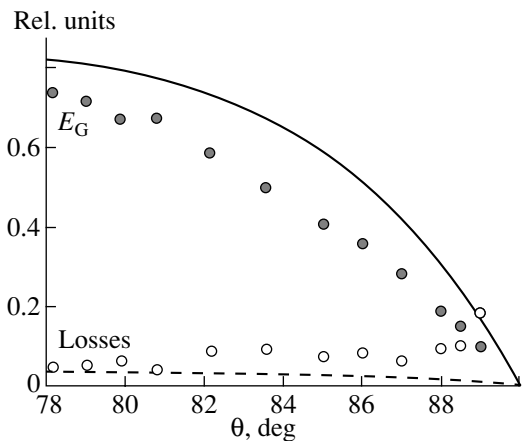


Fig. 7. Gold-coated diffraction grating efficiency E_G and losses vs. radiation incidence angle θ .

where E_0 is the energy emitted on the principal frequency and $E_{\pm\delta\nu}$ are the aside longitudinal mode energies. Equations (7) were solved numerically. The parameters of the laser crystal are presented in the table.

2.2. Modeling Results

In Fig. 4 are shown the laser efficiency η (solid lines) and line-width factor S (dash lines) as a functions of the grating incidence angle θ . Calculations were carried out for $L^{\text{cav}} = 15$ cm, grating length $L_G = 6$ cm, and different transverse diameters of the active region in the laser crystal. As shown, with an increase in the incidence angle, the laser efficiency falls. Firstly, this is due to a decrease in the grating efficiency (see Fig. 7). Secondly, at high incidence angles, the grating input aperture became smaller than the active region transverse size, leading to additional losses. The principal longitudinal mode begins to dominate in the laser emission spectrum at the close-to-limit incidence angles. However, even near the lasing threshold, the principal mode accumulates only 50% of the laser output.

Our calculations have shown that the SLM laser operation can be reached if the cavity length is less than 7 cm (mode spacing >2 GHz) and the diameter of the

active region is less than 0.5 mm. However, experimental realization of the color-center laser with such parameters is rather difficult. The GIG laser cavity with a standard metal-coated diffraction grating has a low Q -factor; therefore, the 4- to -8-cm-long crystal should be used for effective pump radiation conversion. This leads to a minimal cavity length of about 10–15 cm. Moreover, the formation of an active region with a diameter smaller than 1 mm in the laser crystal is also difficult mostly because of the high risk of damage to the metal-coated grating by the pump radiation.

The standard way to improve the GIG cavity spectral selectivity is the use of an intracavity prism-beam expander. The intracavity beam expander makes it possible to increase the selectivity in proportion to its magnification. The drawbacks of using the expander are the extra losses and undesirable lengthening of the laser cavity. In Fig. 5 are shown the laser efficiency η and line-width factor S for the GIG cavity with a beam expander as functions of the grating incidence angle θ . Calculations were carried out for different expander magnifications. The cavity parameters were the same as for Fig. 4, and the diameter of the laser active region was 1 mm. From the figure it follows that the use of the $4\times-8\times$ beam expander makes it possible to reach the SLM laser operation ($S \rightarrow 1$) at incidence angles of about $88.5^\circ-89^\circ$. With this, the laser efficiency does not exceed 1%.

3. EXPERIMENTAL RESULTS

3.1. Laser Crystal

The color-center laser characteristics are strongly dependent on the technology of laser crystal fabrication. One of the most important criteria of the active element quality is the proportion of the active color centers to parasitic color centers in the crystal. Such parasitic color centers cause absorption and additional losses at the pump laser wavelength and the color-center laser wavelength. In the case of the LiF:F_2^- laser, the parasitic color centers are the F_3^- color centers with maximum absorption at 810 nm and aggregate color centers with an absorption band in the 1150- to 1200-nm region.

The spectra of the LiF:F_2^- laser crystals are shown in Fig. 6. As follows from the figure, the maximum values of absorption of the F_2^- centers (at 960 nm) and the F_3^- centers (at 800 nm) are approximately equal. Such a proportion between the concentrations of F_2^- and F_3^- centers allows us to neglect the absorption of F_3^- color centers at the pump laser wavelength, 1064 nm (see dashed parts in the curves in Fig. 6). The spectral tests of 3-cm-long crystals did not fetch out any additional bands corresponding to the absorption of aggregate color centers. This allows us to use the value 0.01 cm^{-1} as an upper estimate for the absorption of aggregate

LiF:F_2^- color-center crystal parameters were used for the simulations

N	3×10^{16}	cm^{-3}
$\sigma_P^{(01)}/\sigma_P^{(10)}$	$1.9 \times 10^{-17}/4.5 \times 10^{-17}$	cm^2
$\sigma_L^{(01)}/\sigma_L^{(10)}$	$0.1 \times 10^{-17}/7.3 \times 10^{-17}$	cm^2
K_P, K_L	0.01	cm^{-1}
τ	55	ns
L_C	6	cm

color centers. For our experiments, we used 4-cm-long a Brewster-angle-cut LiF:F₂⁻ crystal.

3.2. Grating and Expander

In our experiments, we used the standard gold-coated holographic diffraction grating. The frequency of the grating grooves was 1200 mm⁻¹, and the grating length was 6 cm. In Fig. 7, the grating diffraction efficiency is shown as a function of the angle of incidence. Experimental measurements results are shown by circles, and the theoretical figures for the grazing incidence-optimized gold-coated grating are shown by solid lines. As shown, the measured diffraction efficiency is approximately 10% below and the grating losses 5% above the theoretical limits.

A small-size, double-prism beam expander with 4× magnification was mounted in the laser cavity. The expander dimensions were 10 × 10 × 12 mm, and the input aperture was about 1 mm. The expander prisms were made of TF-4 optical glass (ref. index 1.73). The back sides of the prisms were AR coated. The expander transmission was about 98% (approximately 1% below the theoretical limit for the expander with such magnification).

3.3. Pump Laser

The pump source of the color-center laser was a pulsed Nd:YAG laser with passive Q switch. As the Q-switch element was used, the LiF:F₂⁻ crystal had an initial transmission of about 16%. The pump pulse repetition rate was 12–25 Hz, the pump pulse energy was 10–30 mJ, and the pump pulse duration was 25 ns.

3.4. Line-Width Measurements

The spectral characteristics of the color-center laser were measured using a Fabri-Perout interferometer (Burleigh, model RC-110). The second harmonic of the fundamental laser radiation was used for measurements. The interferometer base was variable from 2 to 150 mm. The fines of the interferometer were equal to 6 (measured using a single-frequency He-Ne laser). As the nonlinear element for second harmonic conversion, the KDP crystal was used. This nonlinear crystal has broad-band synchronism in the spectral region of LiF:F₂⁻ laser generation (300 Å/cm). Therefore, the spectral shape of the LiF:F₂⁻ laser pulse can be measured via second harmonic radiation with sufficient accuracy. The interference pattern was registered by a CCD array.

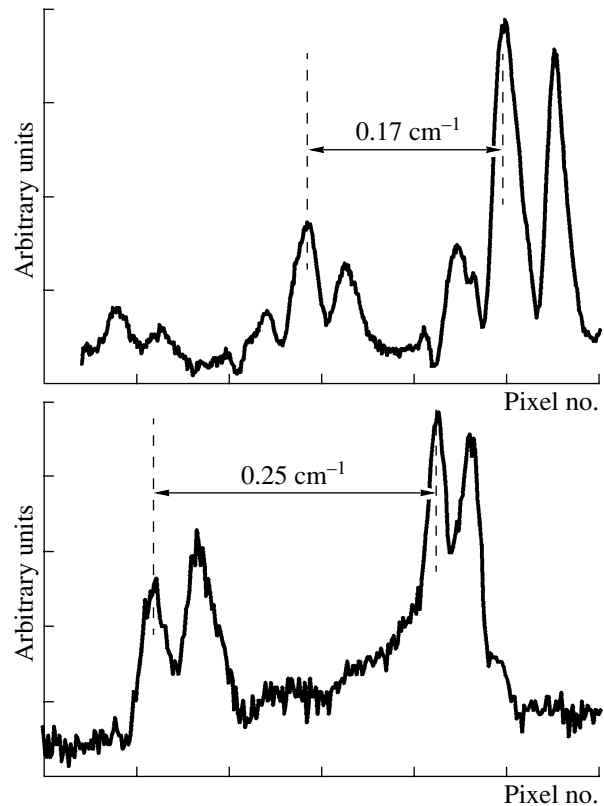


Fig. 8. Interference patterns for multiple-longitudinal mode laser emission.

3.5. Experimental Results

The standard layout of the GIG cavity laser is shown in Fig. 1. At a LiF:F₂⁻ crystal length of about 4 cm and a grating length of about 6 cm, the cavity optical length was approximately equal to 14 cm, which corresponds to a cavity mode spacing of 0.04 cm⁻¹. The grating incidence angle was variable in the range 85°–88°. The pump laser beam was focused in the laser crystal through a lens with a focal length of 30 cm. The average transverse diameter of the pumping region in the active crystal was about 2 mm.

At a grating incidence angle of 85°, the laser efficiency was 5%, and at the laser emission line -width, was about 0.08–0.12 cm⁻¹. This corresponds to the laser operation of 2–3 longitudinal modes. The interference patterns for the multimode lasing are shown in Fig. 8. The SLM laser operation was reached for a grating incidence angle of about 89°. At this angle, the laser efficiency was equal to approximately 0.1%. These experimental results are in good agreement with the theoretical estimations (see Fig. 5).

To improve the cavity spectral selectivity while keeping an acceptable laser efficiency, the cavity mirror M2 was replaced by a second diffraction grating in a Littrow mounting. For this cavity scheme, the SLM laser operation was reached at a grating incidence angle

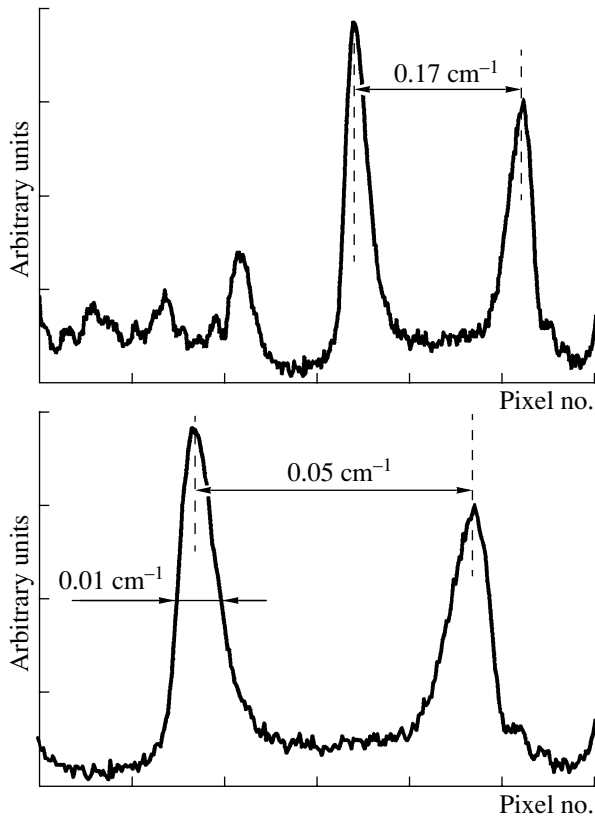


Fig. 9. Interference patterns for single-longitudinal mode laser emission.

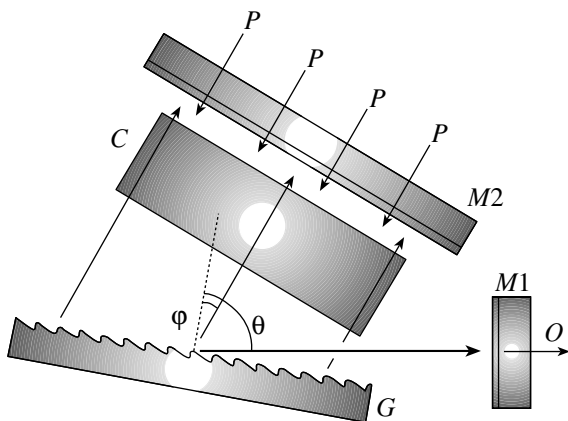


Fig. 10. Novel scheme for the high-power narrowband color-center laser.

of about 86° – 87° , at which the laser efficiency was 0.5–1% at a pump pulse energy of about 20 mJ. The interference patterns for the SLM lasing are shown in Fig. 9. As follows from the figure, the laser emission line width does not exceed the Fabry–Perout resolution (0.01 cm^{-1}).

4. PROSPECTIVE SCHEME OF THE LASER CAVITY FOR THE HIGH-POWER NARROW-BAND COLOR-CENTER LASER

The presented theoretical and experimental results demonstrate two drawbacks of the standard GIG cavity scheme. Firstly, low efficiency of the diffraction grating in a grazing incidence mounting limits the laser efficiency. Secondly, the small input aperture of the grating in a grazing incidence mounting limits the transverse size of the laser active region and, hence, the maximum output power of the laser.

The GIG laser efficiency can be significantly improved by using dielectric diffraction structures instead of a metal-coated grating. In papers [7–9], the combination of the dielectric diffraction grating with the metal of a multilayer dielectric mirror was proposed and studied. In particular, it was shown that the efficiency of the combined grating in a grazing incidence can be close to the 100% limit.

However, the use of a highly effective dielectric diffraction grating does not solve the problem of the laser output power scaling upward. In a standard GIG cavity configuration (see Fig. 1), the diameter of the active region (and hence the output power of the laser) is limited by the aperture of the grating. For the 6-cm-long grating and an incidence angle of 89° , the grating aperture is $a = L_G \cos \theta \approx 1 \text{ mm}$, which limits the maximum pump pulse energy by a few mJ. Moreover, even small transverse displacements of the active region position ($\sim \lambda \cos \theta$) can cause hops in the laser mode. Thus, for the realization of the SLM color-center laser with stable characteristics, a highly stable and high-output-beam-quality pump laser should be used.

To realize the high-power narrowband color-center laser, we propose the novel grazing incidence grating cavity scheme shown in Fig. 10. In contrast with the standard GIG cavity scheme, the active element is placed toward the wider cavity arm (between the grating G and mirror M2). The pump radiation couples in the laser crystal via the dichroic mirror M2. To form active region with the required geometry, the cylindrical optics or the prism beam expander or transverse pumping scheme can be used. Displacement of the active element toward the wider cavity arm makes it possible to significantly increase the pump power and reduce the requirements on the spatial stability of the pump laser beam. In particular, several pump lasers can be used.

The effectiveness of the proposed cavity scheme was examined experimentally. In the first series of experiments, the laser crystal was pumped by a narrow beam. To simulate the wide-beam pumping, the prism beam expander was placed between the mirror M2 and the grating G. The cavity optical length was about 20 cm. At grating incidence angles of 87° and 88.5° , the laser line widths of about 0.2 and 0.1 cm^{-1} , respectively, were reached.

In the second series of experiments, the wide aperture active element with prism geometry was used. Such geometry allowed us to incorporate the active element and intracavity beam expander and decrease the cavity length to 12 cm. Simultaneously, the external pump beam expansion was used. As a result, the transverse size of the active region in the laser crystal was variable in the 3- to -30-mm range. At a grating incidence angle of about 87°, the laser line width was equal to approximately 0.15 cm⁻¹ and did not change with variation in the pump beam size. SLM laser operation with an efficiency of about 0.1% was reached when the etalon was placed in the laser cavity. Thus, our experiments have shown that the proposed scheme provides laser efficiency and spectral selectivity comparable with the standard cavity configuration.

5. CONCLUSIONS

A theoretical and experimental study of the LiF:F₂⁻ color-center laser with a GIG cavity was carried out. The developed mathematical model of the laser allowed us to estimate the laser spectral and energy parameters. It was shown that the use of the simplest GIG cavity scheme (without intracavity expanders or etalons) does not make it possible to reach SLM laser operation. This is caused by the low diffraction efficiency of the available metal-coated diffraction gratings in a grazing incidence mounting and the necessity of using laser crystals that are several centimeters long (long cavity with small mode space <1 GHz).

The calculations made for the GIG laser with an intracavity beam expander have shown that the SLM laser operation can be reached for an expander magnification of 4×–8× at grating incidence angles of about 89°. With this, the laser efficiency does not exceed a fraction of a percent. The experimental measurements of the color-center laser parameters with a 4× beam expander are in good agreement with the simulation results.

To increase the laser efficiency, one of the cavity mirrors (mirror M2 in Fig. 1) was replaced by the second diffraction grating in the Littrow configuration.

This allowed us to reach SLM laser operation at a primary grating incidence angle of about 87° and increase the laser efficiency up to 1%.

Our theoretical and experimental investigations have shown that the important drawback to using the standard GIG cavity scheme for the realization of an SLM LiF:F₂⁻ color-center laser is the small aperture of the diffraction grating at the close-to-limit incidence angles. It limits the maximum pump pulse energy by few tens of mJ. To overcome this problem, we have proposed and experimentally tested the novel scheme of a GIG laser cavity. The proposed scheme allows us to scale up the pump power and significantly decreases the requirements on the quality of the pump laser beam. The use of the proposed cavity scheme is most prospective in combination with a highly effective dielectric diffraction grating.

ACKNOWLEDGMENTS

This work was partly supported by RFBR project no. 01–02–16309a, ISTC and EOARD partner project no. 2022p, and by the Russian Ministry of Industry, Science, and Technology in the framework of the program “Fundamental Spectroscopy,” project M3–03.

REFERENCES

1. M. G. Littman and H. J. Metcalf, *Appl. Opt.* **17**, 2224 (1978).
2. S. V. Vassiliev, V. A. Mishin, and T. V. Shavrova, *Quantum Electron.* **27**, 126 (1997).
3. B. Pati and J. Borysow, *Appl. Opt.* **36**, 9337 (1997).
4. F. J. Duarte and J. A. Piper, *Appl. Opt.* **20**, 2113 (1981).
5. M. G. Littman and J. Montgomery, *Laser Focus* **24** (2), 70 (1988).
6. T. T. Basiev, P. G. Zverev, A. G. Papashvili, and V. V. Fedorov, *Quantum Electron.* **24**, 591 (1997).
7. A. S. Svakhin, V. A. Sychugov, and A. E. Tikhomirov, *Zh. Tekh. Fiz.* **61**, 124 (1991).
8. S. V. Vassiliev, *Quantum Electron.* **25**, 416 (1998).
9. S. V. Vassiliev and V. A. Sychugov, *Quantum Electron.* **31**, 72 (2001).